Comprehensive *ab initio* study of effects of alloying elements on generalized stacking fault energies of Ni and Ni_3Al

Heyu Zhu [1,2] Jiantao Wang,[1,2] Yun Chen,[1] Mingfeng Liu,[1,2] Hui Ma,[1] Yan Sun,[1] Peitao Liu [1,*] and Xing-Qiu Chen [1,†]
[1]*Shenyang National Laboratory for Materials Science, Institute of Metal Research, Chinese Academy of Sciences, 110016 Shenyang, China*
[2]*School of Materials Science and Engineering, University of Science and Technology of China, 110016 Shenyang, China*

(Received 6 January 2023; revised 8 March 2023; accepted 28 March 2023; published 11 April 2023)

Excellent high-temperature mechanical properties of Ni-based single-crystal superalloys (NSCSs) are attributed to the yield strength anomaly of Ni_3Al that is intimately related to generalized stacking fault energies (GSFEs). Therefore, clarifying the effects of alloying elements on the GSFEs is of great significance for alloys design. Here, by means of *ab initio* density functional theory calculations, we systematically calculated the GSFEs of different slip systems of Ni and Ni_3Al without and with alloying elements using the alias shear method. We obtained that for Ni, except for magnetic elements Mn, Fe, and Co, most of the alloying elements decrease the unstable stacking fault energy (γ_{USF}) of the $[01\bar{1}](111)$ and $[11\bar{2}](111)$ slip systems and also decrease the stable stacking fault energy (γ_{SF}) of the $[11\bar{2}](111)$ slip system. Interestingly, the reduction effects exhibit a strong correlation with the inverse of atom radii. For Ni_3Al, most of the alloying elements in groups IIIB–VIIB show a strong Al site preference. Except for Mn and Fe, the elements in groups VB–VIIB and the first column of group VIII increase the values of γ_{USF} of different slip systems of Ni_3Al, which makes the slip deformation and dislocation emits difficult. On the other hand, the elements in groups IIIB–VIIB also increase the value of γ_{SF}, and thus reduce the stability of the antiphase boundary, complex stacking fault, and superlattice intrinsic stacking fault of Ni_3Al. We found that Re is an excellent strengthening alloying element that significantly increases the slip barrier of the tailing slip process for Ni, and also enhances the slip barrier of the leading slip process of three slip systems for Ni_3Al. W and Mo exhibit similar effects as Re. We predicted that Os, Ru, and Ir are good strengthening alloying elements as well, since they show the strengthening effects on both the leading and the tailing slip process for Ni and Ni_3Al. This work established an exhaustive dictionary of the effects of various alloying elements on the GSFEs of both Ni and Ni_3Al phases, which would help to guide the design of next-generation high-performance NSCSs.

DOI: 10.1103/PhysRevMaterials.7.043602

I. INTRODUCTION

Nickel-based single-crystal superalloys (NSCSs) exhibit excellent mechanical properties due to the formation of a large volume fraction of ordered Ni_3Al precipitates that are coherently embedded in the matrix of the Ni phase [1–4]. These ordered precipitates lead to order strengthening and anomalous temperature dependence of yield strength, thereby resulting in extraordinarily high strength and creep resistance at elevated temperatures [3].

As an intrinsic property of the materials with the $L1_2$ structure [5,6], the yield strength anomaly (YSA) is intimately connected to the stacking faults (SFs) in the (111) plane of Ni_3Al, including the antiphase boundary (APB), the superlattice intrinsic stacking fault (SISF), and the complex stacking fault (CSF) [7]. For example, it was found that the thermally activated cross-slip of screw dislocations from the {111} primary slip plane to the {001} cross-slip plane is responsible for the YSA occurrence [8,9], since the cross-slip remains locked in Kear-Wilsdorf (KW) configurations [9]. The driving force to form the KW locks was found to be positively correlated with the APB energy (γ_{APB}) [10] according to the Paidar-Pope-Vitek model [11]. Moreover, the KW locks tend to form when the CSF energy (γ_{CSF}) is low [5,12]. Furthermore, the dislocation ribbons of overall Burgers vector $[\bar{1}12]$ shearing the Ni_3Al precipitates can also affect the YSA [13–16]. Specifically, at intermediate temperatures and high stresses, the $[1\bar{1}0]$ dislocations first form in the matrix of the Ni phase and then decompose at the Ni/Ni_3Al interface at the end of the first stage of creep or at the beginning of the second stage of creep [14]. The decomposition reaction can be described by $1/2[011] + 1/2[\bar{1}01] \rightarrow 1/3[\bar{1}12] + 1/6[\bar{1}12]$ [14]. The leading partial dislocation $1/3[\bar{1}12]$ enters the Ni_3Al phase and creates a SISF, while the tailing partial dislocation $1/6[\bar{1}12]$ remains at the Ni/Ni_3Al interface [14]. The formation of the $[\bar{1}12]$ dislocation ribbons was first observed by Leverant and Kear using transmission electron microscopy [17] and later confirmed by other studies [14,15,18,19]. The SISF has a lower energy as compared to other SF configurations and was thought to be the dominant SF that drives the shearing of the Ni_3Al phase under high stress and intermediate-temperature creep conditions [14,20–23]. In addition, the formation of high-density SFs can promote the accumulation of partial dislocations, thereby

*ptliu@imr.ac.cn
†xingqiu.chen@imr.ac.cn

enhancing both the ductility and fracture toughness but without compromising high strengths. Considering the significant effects of the SFs in improving the creep behavior of NSCSs, controllable tuning the SF energy by alloying would be highly desirable for the design of high-performance NSCSs.

Experimentally, it is tough to obtain an accurate value of the SF energy of NSCSs, because the separation distance between partial dislocations in electron microscope images is too small to identify [24,25]. Based on the weak-beam method of electron microscopy, the derived SF energies of the Ni phase normally lie in the range of 120–130 mJ/m^2 [26,27]. It is well known that to acquire high-performance NSCSs, more than ten alloying elements have been added to the NSCSs so far, such as Ti, V, Cr, Co, Zr, Nb, Mo, Ru, Hf, Ta, W, and Re. For instance, it was experimentally found that Re and Co can reduce the SF energy of Ni [28]. Similar effects were obtained by other alloying elements such as Co, Cr, Mo, Ti, and W [29,30].

In contrast to experiments, theoretical calculations, in particular the *ab initio* calculations based on the density functional theory (DFT), have demonstrated their increasing power in alloys design, providing important complementary perspectives in guiding the experimental studies [31–34]. As early as in the year of 1968, Vitek proposed the generalized stacking fault energy (GSFE) model to explain the effect of SF energy on shear deformation [35]. In this model, the local minimum and maximum of the GSFE along the pathway of the slip system are regarded as stable stacking fault energy (γ_{SF}) and unstable stacking fault energy (γ_{USF}), respectively. In general, the low γ_{SF} can lead to a larger width of stacking faults [36], a higher strain-hardening coefficient [37], a higher twinnability [38,39], a lower twinning stress [40], and a lower occurrence of cross-slip (or climb) [27,41] as well as a lower steady-state creep rate [42–44]. The GSFE model combined with *ab initio* calculations has been widely adopted to study the effects of the alloying elements on the SF energies of Ni and Ni_3Al [44–53]. For instance, Yu and Wang [44] found that Mo, Re, and W remarkably decrease the γ_{SF} of Ni due to the *d*-*d* orbital hybridizations between a solute and Ni. Shang *et al.* [45,46] obtained that almost all the alloying elements decrease the γ_{SF} of Ni, with the effect being more pronounced as the alloying element is far from Ni in the periodic table.

Although the effects of alloying elements on the SF energies of the Ni phase have been extensively studied [44–53], they are normally done on a case-by-case basis and a systematic and thorough investigation of typical alloying elements in the periodic table is still lacking, in particular for the Ni_3Al phase for which only a few alloying elements' effects on the SF energies have been reported [53]. The contribution of this work is to establish a general and exhaustive dictionary of the effects of various alloying elements on the GSFEs of different slip systems of both Ni and Ni_3Al phases. This not only allows us to identify good strengthening alloying elements, but also enables us to determine alternative alloying elements that exhibit similar strengthening effects. This is what the materials scientists desire and eventually would help to guide the design of the next-generation high-performance NSCSs.

This work is organized as follows. First, the computational model used to compute the GSFEs for various slip systems of the (111) plane of Ni and Ni_3Al is introduced. Then, the GSFEs of the (111) plane of pure Ni and Ni_3Al as well as their corresponding alloys are calculated. The focus is on elucidating the effects of the considered 29 alloying elements on the values of γ_{SF} and γ_{USF} of different slip systems. Finally, conclusions are drawn.

II. METHODS AND COMPUTATIONAL DETAILS

All first-principles calculations were performed using the Vienna *ab initio* Simulation Package (VASP) [54,55]. The generalized gradient approximation [56] parametrized by Perdew-Burke-Ernzerhof was employed for the exchange-correlation functional. The plane-wave cutoff energy was set to 420 eV and the Brillouin zone was sampled by a Γ-centered *k*-point grid with the smallest allowed spacing between *k* points of 0.16 $Å^{-1}$, The convergence criteria for the total energy and ionic forces were set to 10^{-6} eV and 0.01 eV/Å, respectively. The first-order Methfessel-Paxton method [57] with a smearing width of 0.18 eV was used for structure relaxations, whereas the Blöchl-corrected tetrahedron method [58] was used to obtain more accurate total energies. For all the calculations, spin polarization was considered.

To calculate the GSFEs, two approaches for modeling the SFs have been proposed. The first one is the slab shear method [47,59,60] and the other one is the alias shear method [45,46,61,62]. For the slab shear method, the SF is modeled by equally splitting a supercell into two slabs, where the atoms in the bottom slab are fixed, while the atoms in the upper slab undergo a certain displacement along the slip direction. By contrast, in the alias shear method the SF is complemented by an alias shear deformation of a periodic supercell lattice, whereas the atomic positions are still represented by the initial Cartesian coordinates. As compared to the slab shear method, the required supercell for modeling the SF is reduced by a factor of 2 in the alias shear method, significantly decreasing the computational cost. For this reason, the alias shear method was employed to calculate the GSFEs throughout the work.

Figure 1 sketches the SF model using the alias shear method. First, a supercell with lattice vectors of $N_1\boldsymbol{a}$, $N_2\boldsymbol{b}$, and $N_3\boldsymbol{c}$ was built [Fig. 1(a)]. Then, a small vector $\boldsymbol{t}$ along the slip direction (here $\boldsymbol{a}$) was introduced on the lattice vector $N_3\boldsymbol{c}$, which constructs a slip plane in the *ab* plane [see Fig. 1(b)]. Finally, the supercell (including both lattice vectors and atomic positions) was allowed to relax only along the *c* direction, giving rise to a net vector of $\boldsymbol{t}'$ perpendicular to the slip plane. Here, we employed a 96-atom orthorhombic supercell with the lattice vectors of $[11\bar{2}]a_0$, $2[\bar{1}10]a_0$, and $2[111]a_0$ with a_0 being the lattice constant of a conventional fcc unit cell. The length of the lattice vector along the [111] direction ensures to eliminate interactions between periodic stacking fault planes. The GSFE was calculated by

$$\gamma_{GSF} = (E_{GSF} - E_0)/A, \tag{1}$$

where E_{GSF} and E_0 represent the total energies of the supercell with or without the SF, respectively, and A is the area of the slip plane within the supercell. In order to calculate the γ_{GSF} with an alloying element, for $Ni_{95}X$ we substituted one of the Ni atoms in the GSF plane with an alloying element. Meanwhile, we also replaced a Ni atom in the

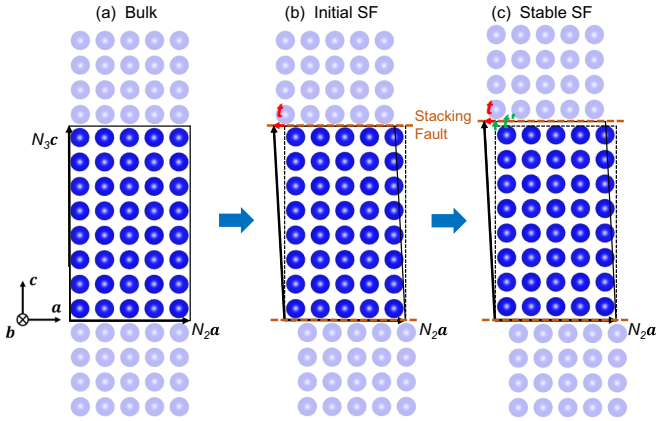

FIG. 1. Sketch of stacking fault (brown dashed lines) modeled by the alias shear method. The lattice containing dark-blue balls indicates the supercell used for calculating the GSFE. (a) Undistorted supercell viewed in the *ac* plane. (b) Initial supercell with an ideal stacking fault, which is created by $N_3\boldsymbol{c} \rightarrow N_3\boldsymbol{c} + \boldsymbol{t}$ with $\boldsymbol{t}$ being a displacement vector along the slip direction (here along $\boldsymbol{a}$). Note that the atomic positions remain fixed in their initial Cartesian coordinates. (c) Supercell after structural relaxations along the c direction only. Here, $\boldsymbol{t}'$ denotes the change of the lattice vector along $\boldsymbol{c}$.

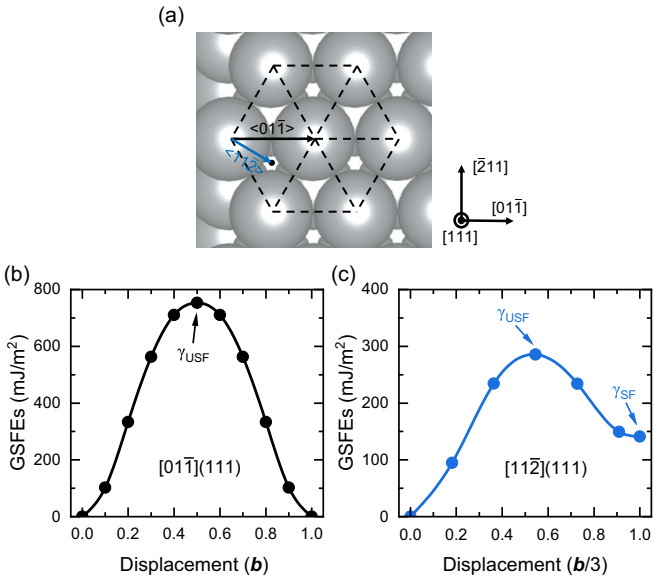

FIG. 2. (a) Sketch of two slip systems of pure Ni, i.e., $[01\bar{1}](111)$ and $[11\bar{2}](111)$. The corresponding GSFEs are shown in (b) and (c).

GSF-free supercell. Since the solute is placed in the stacking fault plane, this translates to a planar solute concentration of 6.25 at.%. A similar procedure was performed for $Ni_{72}Al_{23}X$, but here only the substitution of the Al atom in the GSF plane was considered due to its overall small normalized transfer energy as compared to that when submitting a Ni atom [63–65].

TABLE I. Calculated stable stacking fault energies (γ_{SF}) and unstable stacking fault energies (γ_{USF}) of different slip systems in Ni and Ni_3Al, which are compared to other literature data.

Slip system	γ_{SF} (mJ/m^2)	γ_{USF} (mJ/m^2)	Notes and references
Ni: $[01\bar{1}](111)$		755	Calc., this work, alias shear
		783	Calc., DFT, alias shear [51]
Ni: $[11\bar{2}](111)$	141	285	Calc., this work, alias shear
	160	283	Calc., DFT, alias shear [51]
	149	273	Calc., DFT, slab shear [52]
	129	278	Calc., DFT, slab shear [50]
	120–130		Expt., weak-beam TEM images [26]
Ni_3Al: $[01\bar{1}](111)$	244	819	Calc., this work, alias shear
(APB)	259	830	Calc., DFT, alias shear [51]
	198	791	Calc., DFT, slab shear [52]
	180	778	Calc., DFT, slab shear [48]
	210		Calc., Peierls-Nabarro model [23]
	175±15		Expt., weak-beam TEM images [5]
Ni_3Al: $[\bar{1}2\bar{1}](111)$	214	257	Calc., this work, alias shear
(CSF)	249		Calc., DFT, alias shear [51]
	208	227	Calc., DFT, slab shear [52]
	205	254	Calc., DFT, slab shear [48]
	225		Calc., Peierls-Nabarro model [23]
	235±45		Expt., weak-beam TEM images [5]
Ni_3Al: $[11\bar{2}](111)$	68	1339	Calc., this work, alias shear
(SISF)	47	1421	Calc., DFT, alias shear [51]
	21	1332	Calc., DFT, slab shear [52]
	75	1368	Calc., DFT, slab shear [48]
	80		Calc., Peierls-Nabarro model [23]
	6±0.5		Expt., weak-beam TEM images [5]
	35		Expt., weak-beam TEM images [18]

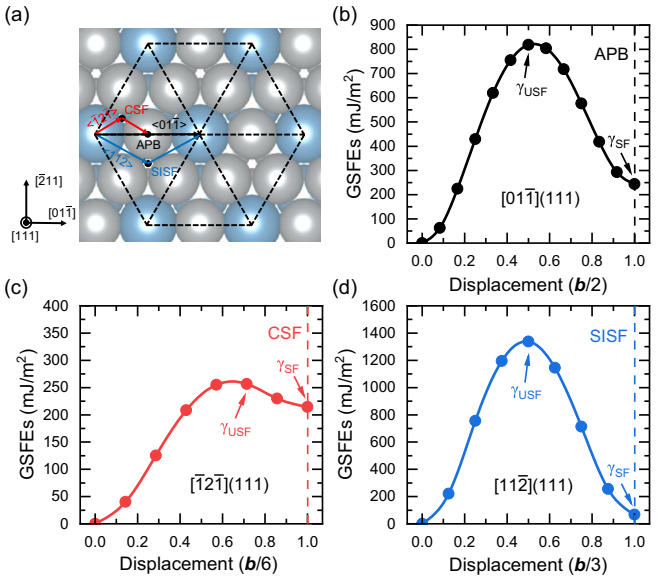

FIG. 3. (a) Sketch of three slip systems of pure Ni_3Al, i.e., [01$\bar{1}$](111), [$\bar{1}$2$\bar{1}$](111), and [11$\bar{2}$](111). The corresponding GSFEs are shown in (b), (c), and (d).

III. RESULTS AND DISCUSSION

A. The GSFEs of pure Ni and Ni_3Al

Let us start from the pure Ni system. For the pure Ni, there are two typical slip systems, i.e., [01$\bar{1}$](111) and [11$\bar{2}$](111) [see Fig. 2(a)]. The corresponding calculated GSFEs are given in Table I and further plotted in Figs. 2(b) and 2(c). The γ_{USF} along the [01$\bar{1}$] direction is computed to be 755 mJ/m^2, which appears at the ***b***/2 Burgers vector, whereas the calculated γ_{USF} along the [11$\bar{2}$] direction appearing at the ***b***/6 Burgers vector is much smaller (285 mJ/m^2). This indicates that launching the [11$\bar{2}$](111) slip system would be easier as compared to the [01$\bar{1}$](111) slip system. This is consistent with the Rice criterion $D = 0.3\gamma_{surf}/\gamma_{USF}$ [γ_{surf} is the surface energy, 1906 mJ/m^2 for Ni(111)] showing that the larger the D value (equivalently smaller γ_{USF}), the more ductile the slip system [66]. Our calculated γ_{SF} and γ_{USF} are overall in line with the literature theoretical and experimental data (see Table I).

Next, we move to the pure Ni_3Al system. For the pure Ni_3Al, three inequivalent slip systems exist on the (111) plane, i.e., [01$\bar{1}$](111), [$\bar{1}$2$\bar{1}$](111), and [11$\bar{2}$](111) [see Fig. 3(a)], due to the symmetry lowering as compared to Ni. Slipping the system along these directions by ***b***/2, ***b***/6, and ***b***/3 Burgers vectors results in the formation of the APB, CSF and SISF, respectively. The corresponding calculated GSFEs are given in Table I and further shown in Figs. 3(b)–3(d). It can be seen that the γ_{USF} for forming the CSF (257 mJ/m^2) is much lower than the γ_{USF} for forming the APB (819 mJ/m^2). These results support the decomposition reaction of a $1/2\langle 1\bar{1}0\rangle$ dislocation into two Shockley partials on the (111) plane of Ni_3Al, which can be described by $1/2\langle 01\bar{1}\rangle \rightarrow 1/6\langle\bar{1}2\bar{1}\rangle + 1/6\langle 11\bar{2}\rangle$ [7] [see red arrows in Fig. 3(a)]. Thus, the [$\bar{1}$2$\bar{1}$] direction exhibits the best ductility. Moreover, the SISF exhibits the smallest γ_{SF} of 68 mJ/m^2, much smaller than those of the APB (244 mJ/m^2) and the CSF (214 mJ/m^2). However, its formation needs to overcome the largest energy barrier (γ_{USF} = 1339 mJ/m^2), where the γ_{USF} decreases in a sequence of [11$\bar{2}$](111) > [01$\bar{1}$](111) > [$\bar{1}$2$\bar{1}$](111). This suggests that once the SISF is produced, it is fairly kinetically stable and its slipping becomes much more difficult. This might be connected with the anomalous temperature dependence behavior of the YSA [14,20–23]. Our predictions are in reasonable agreement with other DFT calculations and experimental estimations (see Table I). The noticeable exception is that the experimentally estimated γ_{SF} of the SISF from Karnthaler *et al.* [5] using weak-beam transmission electron microscopy (TEM) images is somewhat too small (6 ± 0.5 mJ/m^2). However, the more recent experimental estimation by Knowles and Chen [18] using the same technique obtained a much larger value (35 mJ/m^2) that is in better agreement with the DFT calculated results.

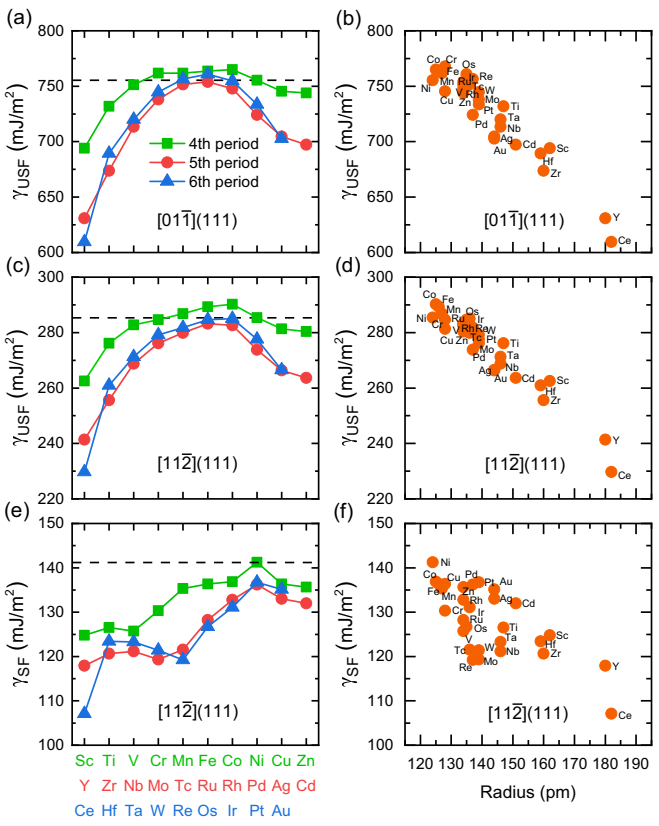

FIG. 4. The effects of the considered alloying elements on the GSFEs of Ni for the slip systems of (a) γ_{USF} of [01$\bar{1}$](111), (c) γ_{USF} of [11$\bar{2}$](111), and (e) γ_{SF} of [11$\bar{2}$](111). (b), (d), and (f) show the corresponding GSFEs as a function of the radii of alloying elements. The dashed line represents the γ_{USF} and γ_{SF} of pure Ni.

B. Effects of alloying elements on the γ_{USF} and γ_{SF} of Ni

To explore the effects of the alloying elements on the γ_{USF} and γ_{SF} of different slip systems in Ni, 29 alloying elements including most of the transition-metal elements and Ce were considered. Figure 4 shows the calculated γ_{USF} and γ_{SF} with the addition of an alloying element on the SF plane. The detailed values are summarized in Table II. First, it is interesting to see that the calculated γ_{USF} for the [01$\bar{1}$](111) and [11$\bar{2}$](111) slip systems exhibit similar

TABLE II. A summary of calculated stable stacking fault energies (γ_{SF}) and unstable stacking fault energies (γ_{USF}) of different slip systems in Ni and Ni_3Al with the addition of alloying elements. The available literature data are also given.

	Ni: $[01\bar{1}](111)$	Ni: $[11\bar{2}](111)$		Ni_3Al: $[01\bar{1}](111)$		Ni_3Al: $[\bar{1}2\bar{1}](111)$		Ni_3Al: $[11\bar{2}](111)$	
Elements	γ_{USF}	γ_{USF}	γ_{SF}	γ_{USF}	$\gamma_{SF}(\gamma_{APB})$	γ_{USF}	$\gamma_{SF}(\gamma_{CSF})$	γ_{USF}	$\gamma_{SF}(\gamma_{SISF})$
Sc	694	263	125 108 [45]	808	280	279	254	1285	132
Ti	732	276	127 113 [45]	841 839 [48]	286	287 308 [48]	260	1352 1438 [48]	131
V	751	283	126 113 [45]	855	289	293	263	1381	131
Cr	768	285 248 [50]	130 119 [46], 110 [51], 107 [45]	855	277	292	261	1385	124
Mn	762	287 274 [47]	135 124 [46], 86[48]	815	215	262	208	1336	82
Fe	764	289 280 [47]	136 125 [46], 86[48]	824	227	268	218	1345	94
Co	765	290 234 [50]	137 127 [46], 110 [51], 124 [45]	824	218	268	215	1347	91
Ni	755	285	141 132 [45]	799	168	247	180	1320	56
Cu	745	281 256 [47]	136 126 [46], 86[48]	785	167	239	172	1298	53
Zn	744	280	136 125 [45]	795	206	246	192	1302	59
Y	631 589 [51]	241 220 [51]	118 96 [46], 130 [52]	778 731 [51]	302 302 [51]	282	273	1211 1083 [51]	159 81 [51]
Zr	674 656 [51]	256 244 [51]	121 101 [46], 135 [52]	820 858 [51]	312 365 [51]	295	283	1286 1350 [51]	155 316 [51]
Nb	713	269 223 [47]	121 104 [46], 59[48]	853	317	304	288	1353	152
Mo	738	276 280 [52]	119 103 [46], 55 [53], 100 [45]	869 1034 [52]	313 531 [52]	308	286	1388 1553 [52]	145 238 [52]
Tc	752	280	122 105 [45]	866	289	304	272	1393	126
Ru	754	283 308 [52]	128 116 [46], 95 [53], 108 [45]	839 905 [53], 837 [49]	233 185 [52]	284 339 [53], 294 [49]	233 242 [52]	1365 1456 [53], 1350 [49]	83 29 [52]
Rh	748	283	133 122 [45]	807	185	264	198	1327	61
Pd	724	274	136 127 [45]	767	151	239	168	1270	46
Ag	705	266	133	756	170	236	175	1241	56
Cd	697	264	132	764	212	244	198	1242	66
Ce	610	230	107	778	331	296	296	1149	177

TABLE II. (*Continued.*)

Elements	Ni: $[01\bar{1}](111)$	Ni: $[11\bar{2}](111)$		Ni_3Al: $[01\bar{1}](111)$		Ni_3Al: $[\bar{1}2\bar{1}](111)$		Ni_3Al: $[11\bar{2}](111)$	
	γ_{USF}	γ_{USF}	γ_{SF}	γ_{USF}	$\gamma_{SF}(\gamma_{APB})$	γ_{USF}	$\gamma_{SF}(\gamma_{CSF})$	γ_{USF}	$\gamma_{SF}(\gamma_{SISF})$
Hf	689	261	123	814	313	295	282	1310	144
	689[51]	253 [51]	106 [46], 140 [52]	914 [51]	373 [51]			1404 [51]	300 [51]
Ta	720	271	123	861	323	306	292	1366	146
		276 [52]	108 [46], 86 [53]	1013 [53], 908 [49]	585 [52]	588 [53], 337 [49]	394 [52]	1479 [53], 1470 [49]	347 [52]
W	745	279	121	881	326	313	295	1404	144
		257[48], 289 [53]	105 [46], 38[48], 59 [53], 103 [45]	1094 [53], 939 [49]	599 [52]	611 [53], 350 [49]	425 [52]	1636 [53], 1531 [49]	281 [52]
Re	757	282	119	884	313	313	287	1413	132
		301 [52]	103 [46], 48 [53], 100 [45]	1079 [53], 941 [49]	494 [52]	524 [53], 366 [49]	432 [52]	1628 [53], 1533 [49]	142 [52]
Os	761	285	127	869	271	303	263	1398	101
			113 [45]						
Ir	755	285	131	828	207	276	215	1353	58
			120 [45]						
Pt	734	278	137	786	163	249	180	1294	40
			128 [45]						
Au	703	266	135	756	165	238	176	1242	48

trends as the atomic number of alloying elements increases along the period [Figs. 4(a) and 4(c)]. Specifically, as the element moves from the left to the right along the period, the γ_{USF} first increases, then reaches the maximum around group VIII elements, and eventually decrease as the atomic number increases further. Second, as compared to Ni, most of the alloying elements tend to reduce γ_{USF} except for Cr, Mn, Fe, Co, Re, and Os [see Figs. 4(a) and 4(c)]. Moreover, the alloying elements in the fifth and sixth periods are found to exhibit more pronounced effects in decreasing γ_{USF} than those in the fourth period. In particular, Ce shows the strongest reduction of γ_{USF}. This indicates that the addition of alloying elements in Ni renders the deformation of $[01\bar{1}](111)$ and $[11\bar{2}](111)$ slip systems more easily.

Moving to the γ_{SF} for the $[11\bar{2}](111)$ slip system, one can observe from Fig. 4(e) that all alloying elements decrease the γ_{SF}, with the effect being more pronounced as the alloying elements are far from Ni in the periodic table. Similar to the effects of alloying elements on γ_{USF}, the alloying elements in the fifth and sixth periods also decrease γ_{SF} more remarkably than the fourth period elements. Although the elements in groups VIB–VIIB and the first two columns of group VIII almost have a negligible effect (just $\pm 2\%$ reduction) on the γ_{USF} along the $[01\bar{1}]$ and $[11\bar{2}]$ directions, they have a considerable effect (about $\pm 15\%$ reduction) on the γ_{SF} of the $[11\bar{2}](111)$ slip system. It is interesting to observe that as compared to the elements in the same period, Mo and Re exhibit an unusual reduction of γ_{SF} due to their *d*-*d* orbital hybridizations with Ni [44]. These results are consistent with the findings of Shang *et al.* [45]. Since a small value of SF results in a low steady-state creep rate [42–44], one can thus expect that the addition of Ce, Y, Re, and Mo in Ni can improve creep resistance and exhibit good solid solution strengthening effect.

Figures 4(b), 4(d) and 4(f) show the calculated γ_{USF} and γ_{SF} of different slip systems as a function of the atomic radii of alloying elements. It is evident that the γ_{USF} follows a linear behavior with respect to atomic radii, and the alloying elements with larger atomic radii in general exhibit a more pronounced reduction effect on γ_{USF}. Among the considered elements, the effects of Y and Ce are strongest, due to their large atomic radii difference with respect to that of Ni. However, for γ_{SF} the degree of linear correlation with atomic radii is relatively decreased. These results suggest that the strain effects induced by alloying elements play a dominant role in reducing the γ_{USF} and γ_{SF} of Ni, which are responsible for the trends manifested in Figs. 4(a), 4(c) and 4(e).

Before closing this section, we make note of the following: We recall that with our employed supercell model the planar solute concentration is 6.25 at.%. Therefore, strictly speaking, our results and discussions apply to the situation of dilute solute concentration. Exploring the effects of solute concentration on the GSFEs is, however, computationally too demanding for all considered 29 alloying elements due to the rapid increase of configuration space, and is beyond the scope of the present work. We shall also stress that in our work we focus only on the general trends of the effects of different alloying elements on the GSFEs of Ni and Ni_3Al. Despite this, it would still be interesting to see to what extent the trends obtained from our calculations in dilute solute con-

centration apply to higher solute concentrations. To this end, we compared our results to the available literature data for Al, Ti, Cr, and Co that were obtained using a relatively small supercell model [45,67] (see Appendix). Since the variations of stacking fault energies were found to almost follow a linear behavior with the solute concentration, the overall trends across different alloying elements remain unchanged with the modification of solute concentrations, i.e., in a sequence of Ti > Cr > Al > Co for reducing the stacking fault energy (see Appendix). In this regard, we can say that the results obtained from our work still have a certain extrapolation capability to the not high solute concentration regime. However, whether this still holds for other alloying elements remains to be carefully examined.

C. Effects of alloying elements on the γ_{USF} and γ_{SF} of Ni_3Al

When an alloying element is added to the ordered Ni_3Al phase, it can substitute either the Ni site or the Al site. Hence, one needs to first determine the site preference of alloying elements before discussing their effects on the γ_{USF} and γ_{SF}. To this end, we employed the Wagner-Schottky model [64,68]. In this model, the site preference can be determined by the normalized transfer energy

$$\widetilde{E}^X_{\mathrm{Ni}\to\mathrm{Al}} = E^X_{\mathrm{Ni}\to\mathrm{Al}}/E_{\mathrm{anti}}, \tag{2}$$

where E_{anti} is the sum of the formation energy of an Al antisite defect and that of a Ni antisite defect. $E^X_{\mathrm{Ni}\to\mathrm{Al}}$ is the transfer energy that an alloying element (X) transfers from a Ni site to an Al site, and at the same time, the Al atom goes to the Ni site that the X atom initially occupied. The transfer energy is defined as

$$E^X_{\mathrm{Ni}\to\mathrm{Al}} = E^X(\mathrm{Al}) + E^{\mathrm{Al}}(\mathrm{Ni}) - E^X(\mathrm{Ni}) - E_{\mathrm{Ni_3Al}}, \tag{3}$$

where $E^X(\mathrm{Al})$ and $E^X(\mathrm{Ni})$ are the total energies of Ni_3Al with an X atom at the Al and Ni sites, respectively, $E^{\mathrm{Al}}(\mathrm{Ni})$ is the total energy of Ni_3Al with an Al antisite, and $E_{\mathrm{Ni_3Al}}$ is the total energy of pure Ni_3Al. According to the Wagner-Schottky model, one can obtain that, if $\widetilde{E}^X_{\mathrm{Ni}\to\mathrm{Al}} < 0$, the solute X has a strong tendency to occupy the Al site, if $\widetilde{E}^X_{\mathrm{Ni}\to\mathrm{Al}} > 1.0$, the solute has a strong tendency to occupy the Ni site, if $0 < \widetilde{E}^X_{\mathrm{Ni}\to\mathrm{Al}} < 0.5$, the solute has a weak Al site preference, and if $0.5 < \widetilde{E}^X_{\mathrm{Ni}\to\mathrm{Al}} < 1.0$, the solute has a weak Ni site preference.

Figure 5 shows the calculated normalized transfer energies of 29 alloying elements. It is evident that Sc, Ti, V, Cr, Y, Zr, Nb, Mo, Tc, Ce, Hf, Ta, W, Re, and Os show a strong Al site preference, while Pd, Pt, and Au exhibit a strong Ni site preference. Mn, Fe, Co, Zn, Ru, and Cd display a weak Al site preference, whereas Cu, Rh, Ag, and Ir show a weak Ni site preference. Our results are consistent with previous studies based on the Wagner-Schottky model [63–65,69,70] and also agree well with the findings of Chen *et al.* [12] using a grand canonical dilute-solution model thermodynamic formalism. In addition, the fact that Ti, Cr, Nb, Ta, W, and Re favor to occupy the Al site in Ni_3Al agrees well with previous fist-principles calculations based Monte Carlo simulations [71,72] as well as the widely accepted experimental recognition [1,73]. We note that the elements with $0 < \widetilde{E}^X_{\mathrm{Ni}\to\mathrm{Al}} < 1$ exhibit a strong composition-dependent site preference. For instance, they prefer to occupy the Ni site in Al-rich Ni_3Al,

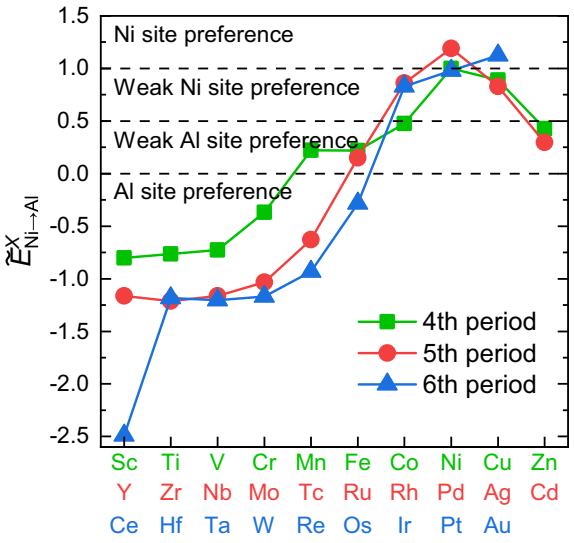

FIG. 5. Calculated normalized transfer energies of 29 alloying elements.

but favor to occupy the Al site in Ni-rich Ni_3Al, while in stoichiometric Ni_3Al they show no site preference such that they randomly occupy the Al and Ni sites [12,49].

Considering that most of the alloying elements tend to occupy the Al site in Ni_3Al, in the following we focus on the effects of the alloying element occupying the Al site on the γ_{USF} and γ_{SF} for three inequivalent slip systems. The results are presented in Fig. 6 and summarized in Table II. It is interesting to find that the effects of alloying elements on γ_{USF} or γ_{SF} follow a similar trend for three slip systems. Taking γ_{USF} for example, when the element moves from left to right in the same period, the γ_{USF} in general first increases, then reaches the maximum, and finally goes down. For the elements in groups VB–VIIB and the first column of group VIII, they have a striking impact on γ_{USF} (except for Mn and Fe) [see Figs. 6(a), 6(c) and 6(e)]. Especially, the elements W and Re in the sixth period and Mo in the fifth period significantly increase the values of γ_{USF}. Since large γ_{USF} values make dislocation emits and plastic deformation more difficult [44], one can expect that the addition of these elements to Ni_3Al can hinder the slip deformation. On the other hand, the elements in groups IB–IIIB and the last column of group VIII have a negative effect on γ_{USF}, in particular the elements Cu, Ag, and Au in group IB, indicating that these elements can improve the slip deformation of Ni_3Al.

For γ_{SF}, the elements in groups IIIB–VIIB (except for Mn) increase γ_{SF}, especially the elements Ce, W, and Re. This means that these elements reduce the stability of the APB configuration in the $[01\bar{1}](111)$ slip system, the CSF configuration in the $[\bar{1}2\bar{1}](111)$ slip system, and the SISF configuration in the $[11\bar{2}](111)$ slip system. Our results are consistent with the findings of Yu *et al.* [44,52]. Since small values of SF lower the steady-state creep rate [42–44], the elements in groups IIIB–VIIB would thus reduce the creep strength of Ni_3Al.

By examining the calculated γ_{USF} and γ_{SF} of Ni_3Al versus atom radii (not shown), we found that they do not simply

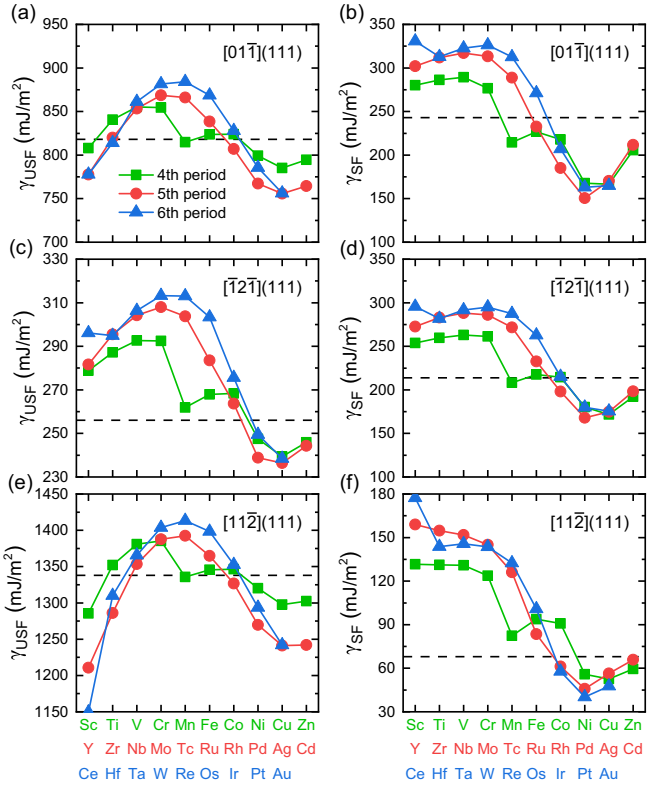

FIG. 6. The effects of considered alloying elements on the γ_{USF} (left panels) and γ_{SF} (right panels) of Ni_3Al for the slip systems of [01$\bar{1}$](111) [(a) and (b)], [$\bar{1}$2$\bar{1}$](111) [(c) and (d)], and [11$\bar{2}$](111) [(e) and (f)]. The dashed line represents the γ_{USF} and γ_{SF} of pure Ni_3Al.

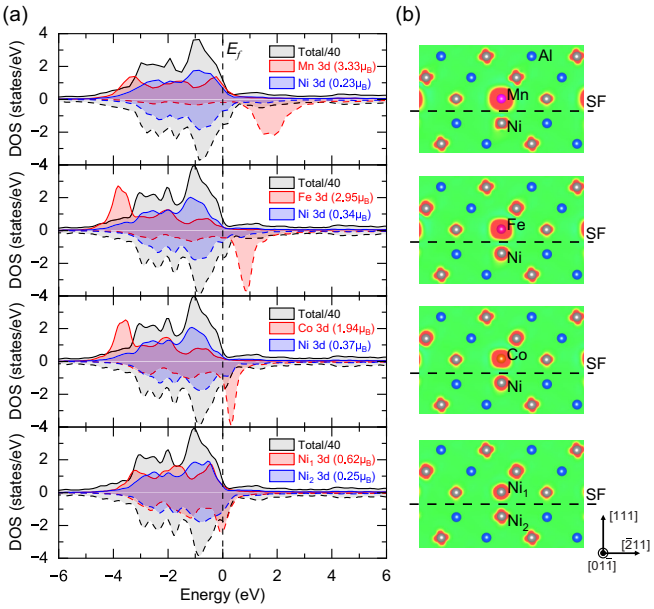

FIG. 7. (a) Spin-polarized local density of states (LDOSs) of alloying elements (Mn, Fe, Co, and Ni) and their first-nearest neighboring Ni atom for the configuration used to calculate the γ_{USF} of the [11$\bar{2}$](111) slip in Ni_3Al. The atomic positions are indicated in (b). The Fermi energy has been aligned to zero. For a better presentation, the total DOSs have been divided by a factor of 40. The values in parentheses represent the calculated magnetic moments. (b) The corresponding spin density isosurface (with an isovalue of 0.01 e/Å^3) for the (01$\bar{1}$) plane including the alloying elements.

follow a linear behavior as is the case in Ni. Thus, besides the strain effects, electronic structures changed by the alloying elements also take effects in determining the values of γ_{USF} and γ_{SF} for Ni_3Al. Furthermore, one notices that among the considered elements, Mn, Fe, and Co exhibit abnormal behaviors (see Fig. 6). Our electronic structure analysis demonstrates that these abnormal behaviors originate from their strong spin polarizations. Just taking the γ_{USF} of the [11$\bar{2}$](111) slip in Ni_3Al as an example, we plot in Fig. 7 the LDOSs of alloying elements (Mn, Fe, Co, and Ni) and their first-nearest neighboring Ni atom as well as corresponding spin density isosurfaces. It is evident that the spin polarization decreases in the order of Mn, Fe, Co, and Ni, yielding local magnetic moments of $3.33\mu_B$, $2.95\mu_B$, $1.94\mu_B$, and $0.62\mu_B$, respectively. By contrast, the other alloying elements do not exhibit magnetic couplings with the neighboring Ni atoms.

D. Effects of alloying elements on normal slip barriers

The slip deformation is a reaction process with an energy barrier (γ_{USF}) to overcome to form stable SFs, whose stability is described by γ_{SF}. In order to better describe the effects of alloying elements on the SFs, here we defined the process from a perfect supercell slip to the formation of a stable SF configuration as the leading slip process (LSP) and its inverse process was defined as the tailing slip process (TSP) [see Fig. 8(a)]. We notice that simply comparing γ_{SF} and γ_{USF} is not sufficient to capture the overall effects of different alloying elements on GSFEs in an accurate manner. To address this issue, we have proposed renormalized $R_1 = \gamma^X_{USF}/\gamma^0_{USF}$ and $R_2 = (\gamma^X_{USF} - \gamma^X_{SF})/(\gamma^0_{USF} - \gamma^0_{SF})$ indices to effectively characterize the effects of alloying elements on the slip barriers of the LSP and TSP, respectively. Here, γ^X_{USF} and γ^0_{USF} represent the unstable stacking fault energies with and without alloying element X, respectively, whereas γ^X_{SF} and γ^0_{SF} denote the stable stacking fault energies with and without alloying element X, respectively. According to this definition, one can obtain that the indices R_1 (R_2) greater than 1 mean that the alloying elements increase the barrier of the LSP (TSP), which makes deformation more difficult. On the contrary, when the indices are less than 1, the deformation becomes easier with the addition of alloying elements. In this way, the different alloying elements with similar effects can well be classified into the same R_1-R_2 quadrant.

The clarification results are compiled in Fig. 8 in terms of R_1 and R_2. From the plot it is evident that among all considered alloying elements Re is an excellent strengthening element that significantly increases the barrier of the TSP of the [01$\bar{1}$](111) slip system for the Ni phase, and also enhances the barrier of the LSP of the [01$\bar{1}$](111), [$\bar{1}$2$\bar{1}$](111), and [11$\bar{2}$](111) slip systems for the Ni_3Al phase. However, it shows a negligible or even slight negative impact on the LSP of the [01$\bar{1}$](111) slip system in Ni and the TSP of the [$\bar{1}$2$\bar{1}$](111) slip system in Ni_3Al. We note that W and Mo exhibit similar effects as Re. The element of Os is almost distributed in the red area (see Fig. 8), which suggests that it shows strengthening effects on both LSP and TSP for Ni and

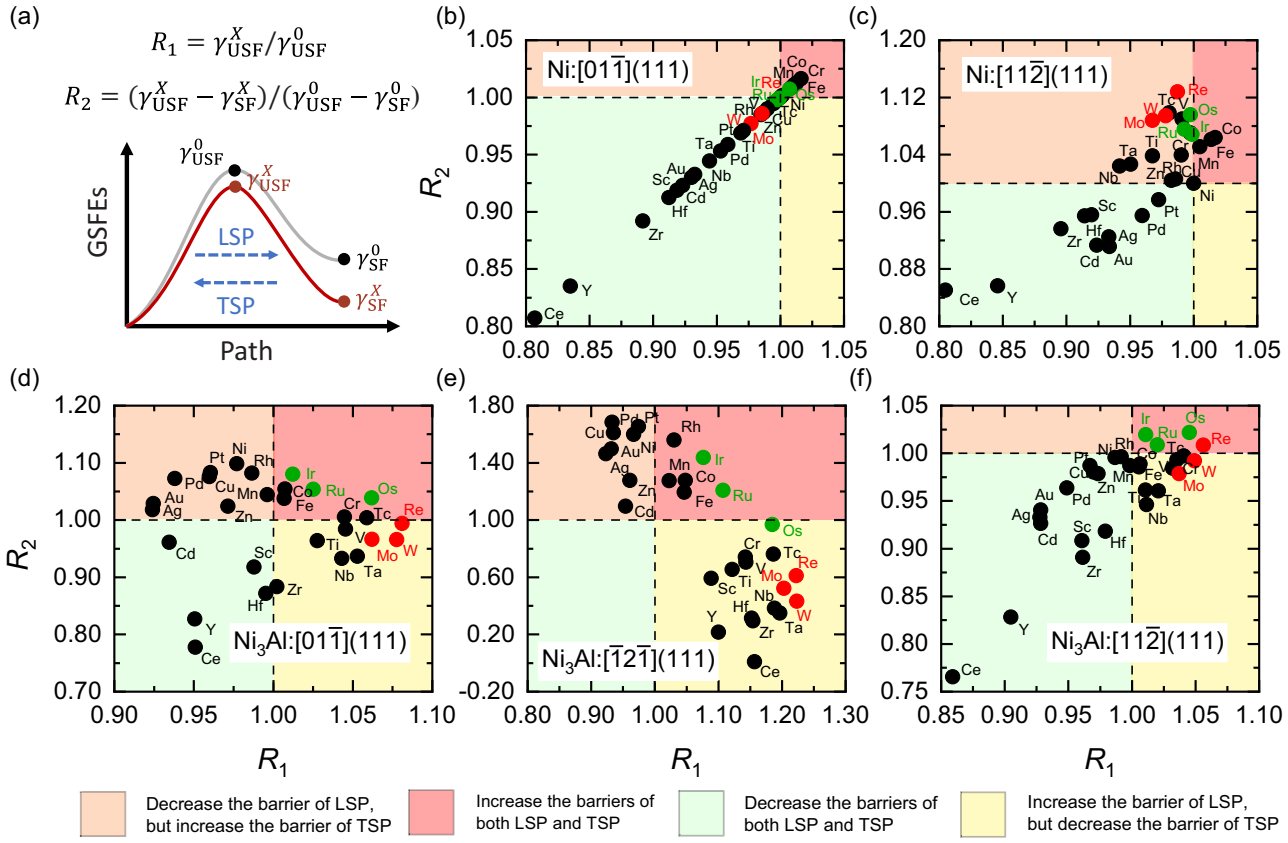

FIG. 8. (a) Sketch of the GSFE curve along a slip path with the LSP and TSP being indicated. (b)–(f) A summary of the effects of alloying elements on the barriers of LSP and TSP for different slip systems in Ni and Ni_3Al. (b) Ni: [01$\bar{1}$](111), (c) Ni: [11$\bar{2}$](111), (d) Ni_3Al: [01$\bar{1}$](111), (e) Ni_3Al: [$\bar{1}$2$\bar{1}$](111), and (f) Ni_3Al: [11$\bar{2}$](111).

Ni_3Al. Our findings are consistent with the design strategy recently proposed by Wei *et al.* [74] who suggested to replace Re by Os in order to improve creep resistance and phase stability of nickel-based single-crystal superalloys. It turns out that the newly designed Os-containing superalloy indeed shows a lower creep rate than the commercial Re-containing CMSX-4 alloy at 980 °C/200 MPa/100 h [74]. In addition, we found that Ru and Ir exhibit similar effects as Os. This might explain why the Ru element has been included in the fourth-generation (EPM-102 [75] and TMS-138 [76]) and fifth-generation NSCSs (TMS-173 [77]), and the Ir element has been included in the sixth-generation NSCSs (TMS-238 [78,79]). By contrast, the rare-earth elements Y and Ce dramatically decrease R_1 and R_2, indicating that they are not good alloying elements for improving the slip barrier of Ni or Ni_3Al. Despite this, a certain amount of Y or Ce has been added to superalloys because of their strong deoxidizing and desulfurizing abilities [80].

IV. CONCLUSIONS

In summary, we have systematically studied the effects of 29 alloying elements on the GSFEs of different slip systems in Ni and Ni_3Al through a comprehensive first-principles calculation based on the alias shear method. The conclusions drawn from this study are as follows:

(i) For Ni, except for magnetic elements Mn, Fe, and Co, most of the alloying elements decrease the γ_{USF} of the [01$\bar{1}$](111) and [11$\bar{2}$](111) slip systems and also decrease the γ_{SF} of the [11$\bar{2}$](111) slip system. The reduction effects show a strong correlation with the inverse of atom radii.

(ii) For Ni_3Al, most of the alloying elements in groups IIIB–VIIB show a strong Al site preference. Except for Mn and Fe, the elements in groups VB–VIIB and the first column of group VIII increase the value of γ_{USF} of different slip systems of the Ni_3Al phase, which makes the slip deformation and dislocation emits difficult. However, the elements in groups IIIB–VIIB also increase the value of γ_{SF}, and thus reduce the stability of the APB, CSF, and SISF configurations of the Ni_3Al phase.

(iii) The alloying elements have been suitably clarified into four quadrants in terms of the two proposed indices R_1 and R_2 (see Fig. 8). We obtained that Re is an excellent strengthening alloying element that significantly increases the slip barrier of the tailing slip process for the Ni phase, and also enhances the slip barrier of the leading slip process of three slip systems for the Ni_3Al phase. W and Mo exhibit similar effects as Re.

(iv) We predicted that Os, Ru, and Ir are also good strengthening alloying elements, which show the strengthening effects on both the leading and tailing slip processes for Ni and Ni_3Al.

We anticipate that our established dictionary of the effects of various alloying elements on the GSFEs of both Ni and Ni_3Al phases and new findings would be appreciated by the broad community for guiding the design of the next-generation high-performance Ni-based single-crystal superalloys.w

ACKNOWLEDGMENTS

This work was supported by the National Key R&D Program of China (Grant No. 2021YFB3501503), the National Natural Science Foundation of China (Grant No. 52188101), the National Science Fund for Distinguished Young Scholars (Grant No. 51725103), and the funding of National Science and Technology Major Project (J2019-VI-0004-0118 and J2019-VI-0019-0134). All calculations were performed on the high performance computational cluster at the Shenyang National University Science and Technology Park.

APPENDIX

In this Appendix, we show in Fig. 9 the variation of stacking fault energies with solutes (Al, Ti, Cr, and Co) for four different planar solute concentrations.

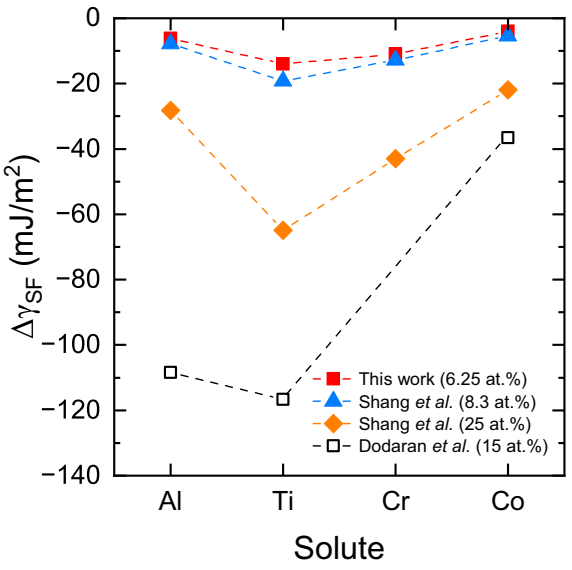

FIG. 9. Variation of stacking fault energies with solutes for four different planar solute concentrations (in parentheses). The available literature data are taken from Refs. [45,67].

[1] R. C. Reed, *The Superalloys Fundamentals and Applications* (Cambridge University Press, Cambridge, UK, 2006).
[2] R. Royce, *The Jet Engine* (Wiley, New York, 2015).
[3] T. Pollock and S. Tin, J. Propul. Power **22**, 361 (2006).
[4] P. Caron and T. Khan, Aerosp. Sci. Technol. **3**, 513 (1999).
[5] H. Karnthaler, E. Mühlbacher, and C. Rentenberger, Acta Mater. **44**, 547 (1996).
[6] Y. Umakoshi, D. Pope, and V. Vitek, Acta Metall. **32**, 449 (1984).
[7] S.-L. Shang, J. Shimanek, S. Qin, Y. Wang, A. M. Beese, and Z.-K. Liu, Phys. Rev. B **101**, 024102 (2020).
[8] G. Schoeck, S. Kohlhammer, and M. Fahnle, Philos. Mag. Lett. **79**, 849 (1999).
[9] Y. M. Wang-Koh, Mater. Sci. Technol. **33**, 934 (2017).
[10] Y. Abate, S. Gamage, L. Zhen, S. Cronin, H. Wang, V. Babicheva, M. H Javani, and M. Stockman, Light Sci. Appl. **5**, e16162 (2015).
[11] V. Paidar, D. Pope, and V. Vitek, Acta Metall. **32**, 435 (1984).
[12] E. Chen, A. Tamm, T. Wang, M. E. Epler, M. Asta, and T. Frolov, npj Comput. Mater. **8**, 80 (2022).
[13] G. Tichy, V. Vitek, and D. P. Pope, Philos. Mag. A **53**, 467 (1986).
[14] C. Rae and R. Reed, Acta Mater. **55**, 1067 (2007).
[15] N. Matan, D. Cox, P. Carter, M. Rist, C. Rae, and R. Reed, Acta Mater. **47**, 1549 (1999).
[16] B. H. Kear, J. M. Oblak, and A. F. Giamei, Metall. Trans. **1**, 2477 (1970).
[17] G. R. Leverant, B. H. Kear, and J. M. Oblak, Metall. Trans. **4**, 355 (1973).
[18] D. Knowles and Q. Chen, Mater. Sci. Eng., A **340**, 88 (2003).
[19] A. Breidi, J. Allen, and A. Mottura, Acta Mater. **145**, 97 (2018).
[20] C. Rae, N. Matan, and R. Reed, Mater. Sci. Eng.: A **300**, 125 (2001).
[21] L. Kovarik, R. Unocic, J. Li, P. Sarosi, C. Shen, Y. Wang, and M. Mills, Prog. Mater. Sci. **54**, 839 (2009).
[22] G. Viswanathan, P. Sarosi, M. Henry, D. Whitis, W. Milligan, and M. Mills, Acta Mater. **53**, 3041 (2005).
[23] O. Mryasov, Y. Gornostyrev, M. van Schilfgaarde, and A. Freeman, Acta Mater. **50**, 4545 (2002).
[24] Y. Qi and R. K. Mishra, Phys. Rev. B **75**, 224105 (2007).
[25] L. Vitos, J.-O. Nilsson, and B. Johansson, Acta Mater. **54**, 3821 (2006).
[26] C. B. Carter and S. M. Holmes, Philos. Mag. (1798–1977) **35**, 1161 (1977).
[27] M. F. de Campos, *Advanced Powder Technology VI*, Materials Science Forum Vol. 591 (Trans Tech Publications Ltd., 2008), pp. 708–711.
[28] S. Ma, L. Carroll, and T. Pollock, Acta Mater. **55**, 5802 (2007).
[29] P. C. J. Gallagher, Metall. Trans. **1**, 2429 (1970).
[30] X. Xie, G. Chen, P. McHugh, and J. Tien, Scr. Metall. **16**, 483 (1982).
[31] R. Li, L. Xie, W. Y. Wang, P. K. Liaw, and Y. Zhang, Front. Mater. **7** (2020).
[32] Y. Ikeda, B. Grabowski, and F. Körmann, Mater. Charact. **147**, 464 (2019).
[33] S. Curtarolo, G. L. W. Hart, M. B. Nardelli, N. Mingo, S. Sanvito, and O. Levy, Nat. Mater. **12**, 191 (2013).
[34] G. L. W. Hart, T. Mueller, C. Toher, and S. Curtarolo, Nat. Rev. Mater. **6**, 730 (2021).
[35] V. Vítek, Philos. Mag. (1798–1997) **18**, 773 (1968).
[36] L. Li, T. Ungár, Y. Wang, J. Morris, G. Tichy, J. Lendvai, Y. Yang, Y. Ren, H. Choo, and P. Liaw, Acta Mater. **57**, 4988 (2009).
[37] D. Pierce, J. Jiménez, J. Bentley, D. Raabe, and J. Wittig, Acta Mater. **100**, 178 (2015).
[38] E. Tadmor and N. Bernstein, J. Mech. Phys. Solids **52**, 2507 (2004).

[39] J. Cahoon, Q. Li, and N. Richards, Mater. Sci. Eng., A **526**, 56 (2009).
[40] V. S. Sarma, J. Wang, W. Jian, A. Kauffmann, H. Conrad, J. Freudenberger, and Y. Zhu, Mater. Sci. Eng., A **527**, 7624 (2010).
[41] M. Chandran and S. K. Sondhi, J. Appl. Phys. **109**, 103525 (2011).
[42] F. A. Mohamed and T. G. Langdon, Acta Metall. **22**, 779 (1974).
[43] A. Argon and W. Moffatt, Acta Metall. **29**, 293 (1981).
[44] X.-X. Yu and C.-Y. Wang, Acta Mater. **57**, 5914 (2009).
[45] S. Shang, C. Zacherl, H. Fang, Y. Wang, Y. Du, and Z. Liu, J. Phys.: Condens. Matter **24**, 505403 (2012).
[46] S. Shang, W. Wang, Y. Wang, Y. Du, J. Zhang, A. Patel, and Z. Liu, J. Phys.: Condens. Matter **24**, 155402 (2012).
[47] D. J. Siegel, Appl. Phys. Lett. **87**, 121901 (2005).
[48] X.-X. Yu and C.-Y. Wang, Mater. Sci. Eng., A **539**, 38 (2012).
[49] N. Eurich and P. Bristowe, Scr. Mater. **102**, 87 (2015).
[50] W. Yang, P. Qu, J. Sun, Q. Yue, H. Su, J. Zhang, and L. Liu, Vacuum **181**, 109682 (2020).
[51] C. Hu, Z. Zhang, H. Chen, J. He, and H. Guo, J. Alloys Compd. **843**, 155799 (2020).
[52] F. Xia, W. Xu, Z. Shi, W. Xie, and L. Chen, Mech. Mater. **165**, 104183 (2022).
[53] X. Zhao, Y. Wang, X. Song, Y. Wang, and Z. Chen, Comput. Mater. Sci. **202**, 110990 (2022).
[54] G. Kresse and J. Furthmüller, Comput. Mater. Sci. **6**, 15 (1996).
[55] G. Kresse and J. Furthmüller, Phys. Rev. B **54**, 11169 (1996).
[56] J. P. Perdew, K. Burke, and M. Ernzerhof, Phys. Rev. Lett. **77**, 3865 (1996).
[57] M. Methfessel and A. T. Paxton, Phys. Rev. B **40**, 3616 (1989).
[58] P. E. Blöchl, O. Jepsen, and O. K. Andersen, Phys. Rev. B **49**, 16223 (1994).
[59] A. Datta, U. Waghmare, and U. Ramamurty, Scr. Mater. **60**, 124 (2009).
[60] J. Han, X. Su, Z.-H. Jin, and Y. Zhu, Scr. Mater. **64**, 693 (2011).
[61] S. Ogata, J. Li, and S. Yip, Science **298**, 807 (2002).
[62] M. Jahnátek, J. Hafner, and M. Krajčí, Phys. Rev. B **79**, 224103 (2009).
[63] A. V. Ruban and H. L. Skriver, Phys. Rev. B **55**, 856 (1997).
[64] C. Jiang and B. Gleeson, Scr. Mater. **55**, 433 (2006).
[65] Q. Wu and S. Li, Comput. Mater. Sci. **53**, 436 (2012).
[66] J. R. Rice, J. Mech. Phys. Solids **40**, 239 (1992).
[67] M. S. Dodaran, S. Guo, M. M. Khonsari, N. Shamsaei, and S. Shao, Comput. Mater. Sci. **191**, 110326 (2021).
[68] K. Badura-Gergen and H.-E. Schaefer, Phys. Rev. B **56**, 3032 (1997).
[69] M. H. F. Sluiter and Y. Kawazoe, Phys. Rev. B **51**, 4062 (1995).
[70] S. Liu, M. Wen, Z. Li, W. Liu, P. Yan, and C. Wang, Mater. Des. **130**, 157 (2017).
[71] H. Zhu, J. Wang, L. Wang, Y. Shi, M. Liu, J. Li, Y. Chen, Y. Ma, P. Liu, and X.-Q. Chen, J. Mater. Sci. Technol. **143**, 54 (2023).
[72] S. B. Maisel, M. Höfler, and S. Müller, Phys. Rev. B **94**, 014116 (2016).
[73] C. Booth-Morrison, Z. Mao, R. D. Noebe, and D. N. Seidman, Appl. Phys. Lett. **93**, 033103 (2008).
[74] B. Wei, Y. Lin, Z. Huang, L. Huang, K. Zhou, L. Zhang, and L. Zhang, Acta Mater. **240**, 118336 (2022).
[75] S. Walston, A. Cetel, R. MacKay, K. Ohara, D. Duhl, and R. Dreshfield, in *Superalloys 2004*, edited by K. A. Green, T. M. Pollock, H. Hiroshi, T. E. Howson, R. C. Reed, J. J. Schirra, and S. Walston (The Minerals, Metals & Materials Society, 2005).
[76] J. Zhang, T. Murakumo, Y. Koizumi, T. Kobayashi, and H. Harada, Acta Mater. **51**, 5073 (2003).
[77] T. Kobayashi, H. Harada, M. Osawa, and A. Sato, J. Jpn. Inst. Met. **69**, 1099 (2005).
[78] T. Yokokawa, H. Harada, K. Kawagishi, T. Kobayashi, M. Yuyama, and Y. Takata, in *Superalloys 2020*, edited by S. Tin, M. Hardy, J. Clews, J. Cormier, Q. Feng, J. Marcin, C. O'Brien, and A. Suzuki (Springer International Publishing, Cham, 2020), pp. 122–130.
[79] K. Kawagishi, A.-C. Yeh, T. Yokokawa, T. Kobayashi, Y. Koizumi, and H. Harada, in *Superalloys 2012*, edited by E. S. Huron, R. C. Reed, M. C. Hardy, M. J. Mills, R. E. Montero, P. D. Portella, and J. Telesman (Wiley, New York, 2012), pp. 189–195.
[80] S. Cao, Y. Yang, B. Chen, K. Liu, Y. Ma, L. Ding, and J. Shi, J. Mater. Sci. Technol. **86**, 260 (2021).